Analytical description of the topological interaction between magnetic domain walls in nanowires

A. Pivano* and V. O. Dolocan†
Aix-Marseille Université, CNRS, IM2NP UMR7334, F-13397 Marseille Cedex 20, France

(Received 22 July 2019; revised manuscript received 22 November 2019; published 27 January 2020)

Magnetic domain walls in nanowires behave as particles interacting through the exchange field. As topological objects, their interaction is determined by their chirality or topological charge. We investigate analytically the topological repulsion between magnetic domain walls with the same topological charge in nanostripes (with easy-plane magnetization) and show that it decays algebraically as r^{-2}, being part of a larger class of interactions that produce topological long-range order in two dimensions. We compare the topological repulsion between the walls with other types of fundamental interactions with exponential spatial decay, such as the Yukawa-Reid potential, and with micromagnetic simulations. We determine that trains of such walls can be well described analytically and can be displaced regularly in nanowires leading to practical applications.

DOI: 10.1103/PhysRevB.101.014438

I. INTRODUCTION

The interaction forces of nature are few and their exact spatial variation is difficult to determine from first principles. In quantum field theory, the fundamental interactions are mediated by massless spin one particles, such as gluons for the strong interaction or photons for the electromagnetic interaction. In the nonrelativistic case, these interactions are described by an interaction potential. In practice, some phenomenological model is often employed as in the case of nucleon-nucleon interaction where a Reid-type (Yukawa) potential is frequently used and compared with experimental results [1]. The Yukawa-type potential is equally used to describe the interparticle interaction in strongly coupled systems, such as ultracooled neutral plasmas [2] as well as in colloidal suspensions [3] (the so-called Yukawa systems).

In several condensed-matter areas and in field theories, the more localized excitations of nonlinear systems are considered as quasiparticles and described within the collective-variable approach [4]. The interactions between these quasiparticles, such as vortices in superconductors, which have an equivalent in cosmology (global strings) [5,6], decay monotonically as r^{-2} in thin superconducting films or exponentially in the bulk [7]. The exponential repulsive interaction is also found in more mundane interactions as the one between two pedestrians [8].

In magnetic systems, the interaction potential is dominated at short range by the exchange interaction. The exchange interaction is model dependent, the most common model being based on the Heisenberg Hamiltonian, from which is derived the semiclassical exchange interaction proportional to the square of the magnetization gradient. This Heisenberg-derived dependence is heavily used in numerical calculations of ferromagnets (micromagnetics) [9].

Domain walls (DWs) confined in magnets on the nanoscale can be considered as particles (macrospins) which interact through the exchange field. The DWs in the confined structures are transverse or vortex DWs depending on the samples dimensions [10]. The DWs are formed from two or more elementary topological defects with an integer winding number, such as vortices in the bulk or fractional winding number which are half-vortices confined to the edges [11,12]. In a planar nanowire with in-plane magnetization (nanostrip), the chirality of the DW is protected by topology and is also called a topological charge [13]. A pair of in-plane DWs with opposite topological charges (opposite fractional edge defects) can be created or annihilated spontaneously, but a pair of DWs with the same topological charge form a stable magnetic texture—a soliton-soliton pair [14] (due to the "topological repulsion," see Fig. 1(a) where four transverse DWs with the same topological charge are pinned in a nanostrip). In a three-dimensional (3D) cylindrical nanowire, it was shown that a pair of DWs with the same initial topological charge form a metastable state that anihilates after a finite time due to the relative rotation of the walls [15] and the nonconservation of the total topological charge. The injection of DWs in a nanowire with reliable chirality control has been demonstrated experimentally [16]. The total topological charge is conserved during DW interaction, and a train of this type of DWs can be displaced jointly in the nanostrip by a polarized current leading to practical applications [17,18].

The interaction potential between the DWs can also be viewed as mediated by the topological defects. The interaction between vortex DWs was studied analytically based on Thiele's approach in a two-dimensional (2D) anisotropic Heisenberg model [19,20] and experimentally [21]. In the majority of cases, only the dynamics of one DW is studied and simulated micromagnetically or the dynamics of well-separated DWs (different nanowires or nanolayers) that interact through the dipolar field [22–31]. In a few cases, the DWs interaction in the same nanowire was studied

*Present address: CEA, DEN, DTN/SMTA/LEAG, Cadarache F-13108 Saint Paul-lez-Durance, France.
†voicu.dolocan@im2np.fr

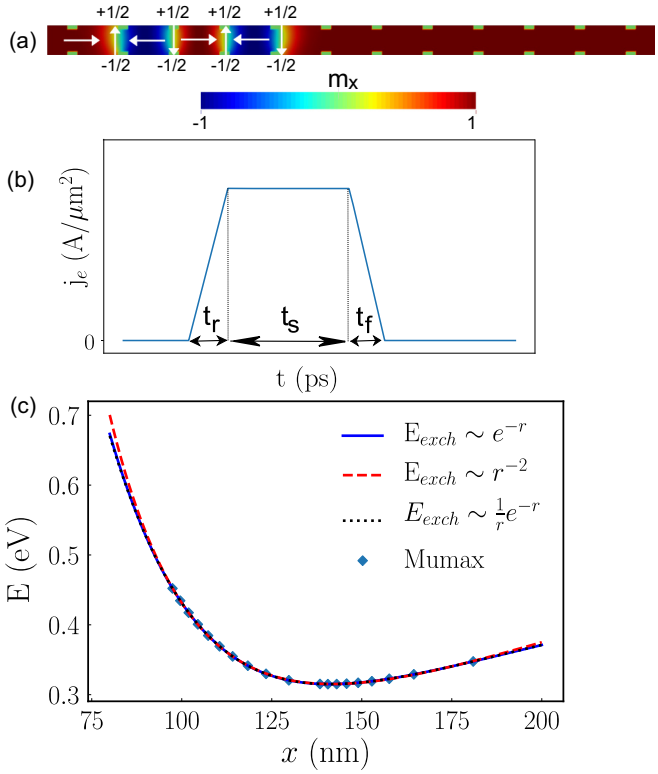

FIG. 1. (a) Simulated structure with four magnetic domain walls with the same topological charge are pinned at symmetric notches: two head-to-head and two tail-to-tail DWs. The fractional winding numbers of the edge defects are indicated for each DW. (b) Current pulse shape used to displace the domain walls. (c) Interaction energy of two domain walls in a nanowire without notches (symbols) as determined from micromagnetic simulations. The curves represent modeling with different trial functions.

experimentally and micromagnetically [32,33]. Analytically, the interaction potential between transverse DWs in nanostripes was considered only based on a the multipole expansion [34], which was tested numerically for DWs pinned at artificial constrictions situated at long distances [15,29,35] where the dipolar interaction dominates. To be able to calculate analytically the dynamics of a train of transverse DWs in a nanowire, a pertinent model should take into account the repulsive (topological) interaction which is important at short range.

In this paper, we address this issue, establishing the transverse DW interaction potential using trial models. We test our phenomenological model numerically on the fast dynamics of two–four transverse DWs initially pinned at symmetric notches along a nanostrip and submitted to ultrashort current pulses. Our analysis is similar to the classical model of a one-dimensional (1D) chain of interacting particles. In our model, we take into account only nearest-neighbor DW exchange interaction and the dipolar interactions up to the third neighbor. We determine that a power-law spatial variation of the DW exchange interaction of r^{-2} type gives quantitatively good results when compared to the micromagnetic calculations, similar with the Heisenberg exchange and the interaction of superconducting vortices in thin films. In a 2D XY model, the interaction between charged particles (vortices) was shown to decrease logarithmically rather than exponentially below a topological phase transition [36]. We compare the obtained power-law behavior with an exponential or a Yukawa potential and discuss the observed differences in the DWs dynamics and depinning currents. We also determine that the transient effects related with the DW inertialike behavior [37–41] due to deformation of the DW diminish when the interaction among several DWs is considered as symmetric interactions on both sides annihilate the deformations of the walls. Our paper shows that a simple analytical model gives good quantitative results even when the interaction among several DWs is considered, paving the way for calculating phase diagrams in larger memory racetracks.

This article is organized as follows. In Sec. II, we present the stochastic 1D model used to calculate the interaction between DWs. In Sec. III, we compute and investigate the phase diagram of the DW dynamics in an infinite nanostrip at $T = 0$ K and at room temperature. Concluding remarks are presented in Sec. IV.

II. MODEL

To determine the interaction potential between transverse magnetic DWs, it is necessary to control the position and the topological charge of the DWs. In the following, the position is controlled by pinning at notches, and the topological charge is fixed initially as the injection with chirality control has already been proven experimentally [16]. The demagnetizing energy keeps the topological charge fixed for the DWs up to reasonable high external applied current. We consider several pinned transverse walls with the same topological charge in an infinite Ni nanostrip (saturation magnetization $M_s = 477$ kA/m, exchange stiffness parameter $A = 1.05 \times 10^{-11}$ J/m, and spin polarization $P = 0.7$) with a cross section of $L_y \times L_z = 60 \times 5$ nm^2. No magnetocrystalline anisotropy is considered, the shape anisotropy ensures that the easy axis is in plane. The strip has rectangular symmetric double notches with dimension $20 \times 9 \times 5$ nm^3 and separated by 80 nm. Figure 1(a) shows the equilibrium position of a train of four neighboring (situated in neighboring notches at 80-nm distance) transverse DWs: two pairs of head-to-head (HH) DWs and tail-to-tail (TT) DWs of the same chirality (and inverse polarity at their centers) to ensure the topological stability and repulsion between them. Each DW sits in a potential well created by the notches [42,43]. The form of the pinning potential was determined from micromagnetic simulations and is presented elsewhere [44] (harmonic at the notches and sinusoidal between them).

The DWs are displaced simultaneously by a series of periodic spin-polarized current pulses applied along the stripe long axis (x direction). The geometry of the current pulse is described in Fig. 1(b): t_r, t_s, t_f, and t_z are the rise, stable, fall time, and zero-current time, respectively. The nonadiabatic parameter is set to $\beta = 2\alpha$, if not specified otherwise.

The DW dynamics was computed using the one-dimensional DW model [22,45] considering the DWs interaction and by 3D micromagnetic simulations with the MUMAX3 package [46]. In both cases, the magnetization dynamics is determined from the Landau-Lifschitz-Gilbert (LLG) equation

with adiabatic and nonadiabatic spin-transfer torques [47],

$$\dot{\mathbf{m}} = -\gamma_0 \mathbf{m} \times \mathbf{H}_{\text{eff}} + \alpha(\mathbf{m} \times \dot{\mathbf{m}}) - (\mathbf{u} \cdot \nabla)\mathbf{m} + \beta \mathbf{m} \times (\mathbf{u} \cdot \nabla)\mathbf{m}, \quad (1)$$

where $\mathbf{m}$ is the normalized magnetization, γ_0 is the gyromagnetic ratio, $\mathbf{u} = \mathbf{j}_e P \mu_B / e M_s$ is the spin drift velocity, P is the spin polarization of conduction electrons, μ_B is the Bohr magneton, and $\mathbf{j}_e$ is the applied current density. No additional exotic torques (such as the ones due to the spin-Hall or Rashba effect) were considered. The temperature is considered in the LLG equation as a thermal field added to the effective field. The thermal field has zero average and is uncorrelated in time and space, and its magnitude is the same as the Gaussian noise introduced in the 1D model below.

The analytical equations of motion used are based on the 1D model of the DW (collective coordinates: average DW center position X and azimuthal angle ψ) [48,49],

$$\begin{aligned}(1+\alpha^2)\dot{X} &= -\frac{\alpha\gamma\Delta}{2\mu_0 M_s S}\frac{\partial E}{\partial X} + \frac{\gamma\Delta}{2} H_k \sin 2\psi \\ &\quad + qp\frac{\gamma}{2\mu_0 M_s S}\frac{\partial E}{\partial \psi} + (1+\alpha\beta)u + \eta_\psi - \alpha\eta_X, \\ (1+\alpha^2)\dot{\psi} &= -qp\frac{\gamma}{2\mu_0 M_s S}\frac{\partial E}{\partial X} - \frac{\gamma\alpha}{2} H_k \sin 2\psi \\ &\quad - \frac{\alpha\gamma}{2\,\Delta\mu_0 M_s S}\frac{\partial E}{\partial \psi} + qp\frac{\beta-\alpha}{\Delta}u + \eta_X + \alpha\eta_\psi,\end{aligned} \quad (2)$$

with $\Delta(t) = \Delta[\Psi(t)] = \pi\sqrt{\frac{2A}{\mu_0 {M_S}^2 \sin^2\psi + \mu_0 M_S H_k}}$ the DW width, H_k as the DW demagnetizing field, η_X and η_ψ represent stochastic Gaussian noise with zero mean value and correlations $\langle \eta_i(t)\eta_j(t')\rangle = (2\alpha k_B T)/(\mu_0 M_s \Delta S)\delta_{ij}\delta(t-t')$. E is the potential energy of the DW that includes the internal energy, the interaction energy with other DWs, and the pinning energy. The azimuthal angle of the DW ψ represents the conjugate momentum in the Lagrangian formulation. The interaction energy between DWs separated by r_{ij} was modeled as $E_{\text{int}} = E_{\text{exch}} + E_{mm} + E_{dd}$, where

$$\begin{aligned}E_{mm}^{ij} &= \frac{a_2 D_2}{r_{ij}} Q_i Q_j, \quad E_{dd}^{ij} = a_3\left(\frac{D_3}{r_{ij}}\right)^3 \cos(\psi_i - \psi_j), \\ E_{\text{exch}}^{H} &= a_1\left(\frac{D_1}{r_{ij}}\right)^2, \quad E_{\text{exch}}^{\text{exp}} = a_1 e^{-r_{ij}/D_1}, \\ E_{\text{exch}}^{Y} &= \frac{a_1 D_1}{r_{ij}} e^{-r_{ij}/D_1}\end{aligned} \quad (3)$$

represent the monopole-monopole (*mm*), the dipole-dipole (*dd*) interaction, and the DW exchange interaction (topological repulsion). The topological charge of the DW is $q = \frac{1}{\pi}\int dx\, \partial_x \psi = \pm 1$ and is related with the direction of rotation of the in-plane magnetization when traversing the DW, and $p = \pm 1$ represents the direction of the magnetization at the DW center along the y axis (width). Although both HHDW and TTDW can have a positive or negative topological charge and direction p, the product $Q = qp$ is always equal to $+1$ for a HHDW and to -1 for a TTDW. Therefore, the *mm* and *dd* interactions between nearest-neighbor HHDW and TTDW of same topological charge but opposite p directions are always negative, meaning attractive. We introduce a repulsion term, in the form of a topological or DW exchange interaction in a phenomenological manner as shown by the E_{exch} terms of Eq. (3). Several trial functions were used and compared based on the asymptotic behavior of fundamental potentials, and the interaction potential which correlates best with the micromagnetic simulations is the r^{-2} decay. We only considered nearest-neighbor DW exchange interaction, but *mm* and *dd* interactions were considered up to the third neighbor (see the discussion on the displacement of the four DWs below).

The parameters a_i and D_i were determined by comparing the obtained phase diagrams with the micromagnetic simulations. As the number of parameters is large, the starting values were chosen by fitting the micromagnetic results obtained for two DWs (a HHDW and a TTDW) initially situated at 80-nm distance in a very long nanowire of the same section and without notches [Fig. 1(c)]. The two DWs repel each other at a closer distance until around an equilibrium position of 140 nm, beyond which the interaction becomes attractive due mainly to the long-range dipolar interaction. These initial parameters were modified in the case of the pinned DWs as to follow closely the micromagnetic phase diagrams, but the order of magnitude was maintained.

For the micromagnetic computations, the strip was discretized into a mesh with a cell size of $2 \times 3 \times 2.5$ nm^3, inferior to the exchange length (∼5 nm). The DW dynamics is studied in an infinity long wire where the magnetic charges at the ends of the nanostrip are compensated.

III. RESULTS

Our analysis of the DWs' dynamical interaction begins with the study of the impact of the different interaction potential trial functions on the phase diagram obtained when a symmetric pulse (stable time t_s—current amplitude j_e) or an asymmetric pulse (rise time $t_r - j_e$) are applied to the pinned DWs at $T = 0$ K. Afterwards, the particularities of the DWs' motion at room temperature are discussed for the different interaction terms. The last subsection details the influence of the transient displacement on the DW dynamics.

A. Influence of the DW exchange energy on the phase diagrams at $T = 0$ K

To evaluate the impact of the different DW exchange terms on the DWs' coupled dynamics, we computed 400×300 point-by-point analytical phase diagrams integrating Eqs. (2) with a fourth-order Runge-Kutta scheme. The phase diagrams represent the relative position of the train of DWs after periodic spin-polarized current pulses are applied to them. The current pulses are varied in length, amplitude, or shape and the correlated displacement of the DWs is extracted after several periodic current pulses. When the DWs are displaced collectively keeping the same relative distance between them, we consider that an expected and desired state is realized. These collective regular displacements form bands depending on the pulse characteristics and the interaction potential between the DWs. The analytical diagrams are compared with the micromagnetic ones (24×31 points). As previously de-

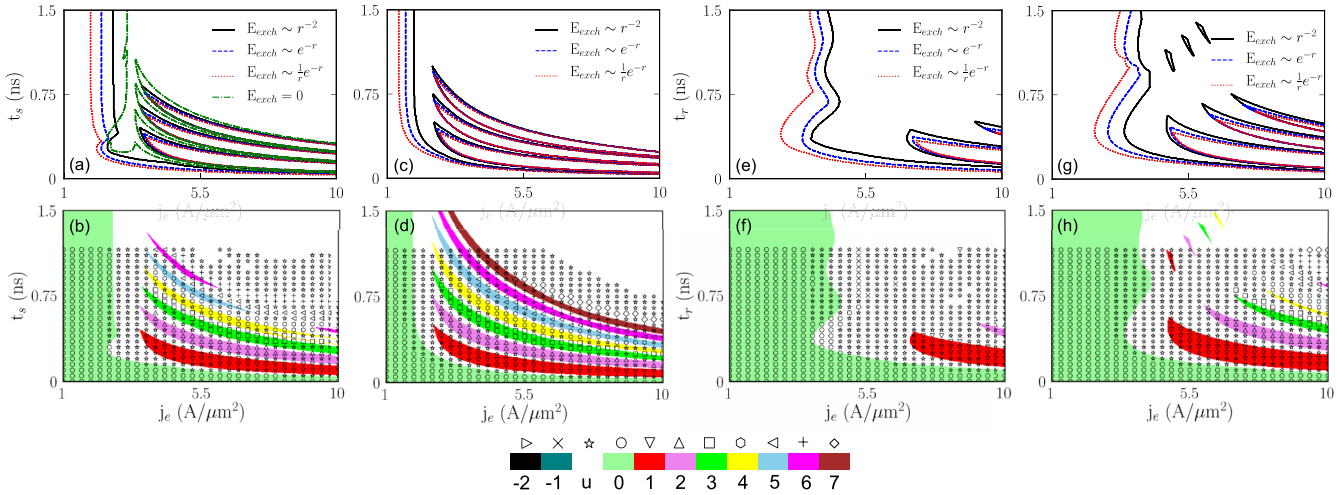

FIG. 2. Contour plots of the different bands obtained for a train of two neighboring DWs with different types of a DW exchange interaction at $T = 0$ K using the 1D model are represented in the upper panels (a), (c), (e), and (g). In the lower panels, the 1D results (colored regions) obtained for a Heisenberg-type DW exchange interaction are compared with the micromagnetic calculations (scattered symbols) for the same pulse characteristics and α and β parameters as the upper panels. The numbering of the bands is as follows: Positive bands correspond to the DWs moving collectively in the direction of the electron flow with the same initial relative distance between them, negative numbers to the DWs moving collectively in the opposing direction with the same initial relative distance between them, the zero state corresponds to the DWs staying pinned at initial positions and "*u*" corresponds to the unintended states in which the DWs do not move synchronously in either direction. The parameters used are as follows: (a) and (b) t_s variable, $t_r = t_f = 5$ ps, $\alpha = 0.02$, $\beta = 0.04$, (c) and (d) t_s variable, $t_r = t_f = 5$ ps, $\alpha = 0.05$, $\beta = 0.1$, (e) and (f) t_r variable, $t_s = t_f = 5$ ps, $\alpha = 0.02$, $\beta = 0.04$, (g) and (h) t_r variable, $t_s = t_f = 5$ ps, $\alpha = 0.05$, $\beta = 0.1$.

termined [44], the range of the current amplitude was chosen ($\lesssim 10$ A/μm^2) as to to have only viscous motion (no precession) for the pulse duration used ($\lesssim 1.5$ ns), which is on the same order of magnitude with access or reading/writing time in possible magnetic memories based on DWs. At high current amplitude or longer pulse duration, an antivortex appears when a DW depins from a notch [50,51]. The antivortex will perturb the systematic motion of the DWs and their mutual interaction. In the results shown below, an antivortex appears only in a few points in the upper right quadrant of the micromagnetic phase diagrams (detailed in Ref. [44]) where the symbols are missing and does not influence our results.

Our analysis starts with a train of a HHDW and TTDW having the same topological charge and situated in neighboring pinning centers (separated by 80 nm). The initial distance between the DWs ensures that their repulsive interaction is still important as determined from their equilibrium positions and Fig. 1(c). In Fig. 2, we present the results for various α and β parameters (corresponding to the Ni values at 0 K and room temperature [52]) and several pulse shapes. In the upper panels, contour plots for the different bands are shown obtained with the 1D model, whereas the lower panels present a superposition of the 1D model diagrams (represented by colors) with the micromagnetic ones (symbols). The two DWs move together after a pulse application due to the spin transfer torque (STT) in the direction of the electron movement, but the final DW position can be in the opposite direction due to the transitory motion (automotion) [37–41]. We indexed the different regions in the phase diagram based on the relative position of the two DWs as follows: We call the state 0 when the DWs stayed in their initial notch (position) after the application of the pulse (pinned case), state $+1$ if the two DWs went to the next notch in the direction of the electron flow (of the STT) keeping the same distance between them or state -1 if the two DWs went to the next notch in the direction opposite the electron flow. The higher number states were indexed in the same way ($+2$ means displacement of both DWs to the second next notch in the STT direction). State *u* is an unintended state (such as depinning of one DW) where the DWs do not keep the initial relative distance between them. This state appears generally as a transition region between the other states. As our calculation is performed on a finite sample of an infinite nanostrip, to be able to compare to the micromagnetic simulations, the number of bands is finite and the upper right region, that shows an unintended state, corresponds to the DW reaching the nanowire (finite sample) end. The states were determined after the application of, at least, four periodic pulses that displace the DWs between their initial position and the desired position back and forth.

As observed in the lower panels of Fig. 2, the 1D model DW repulsive interaction varying in r^{-2} (called the DW Heisenberg exchange) agrees quantitatively with the micromagnetic simulations up to the third band, afterwards a small shift appears. In the upper panels, the contour plots of only the first bands are shown for different repulsive interaction and different material and pulse parameters. In panel (a), for a symmetric pulse shape ($t_r = t_f = 5$ ps) and $\alpha = 0.02$ ($\beta = 2\alpha$), the contour plots obtained with the three types of DW exchange interaction are superposed with the results obtained with no repulsive interaction (dashed-dotted line). As can be observed, even in the absence of the repulsive interaction, the two DWs can still be displaced synchronously due to the periodic pinning potential and the ultrashort pulses, but the depinning current increases to 3.05 A/μm^2 from 2.60 A/μm^2 above $t_s = 0.6$ ns, and the bands increase and are more deformed. This situation is equivalent with the case of two

DWs initially separated by a longer distance than the range of the repulsive interaction (Supplemental Material [53]). The depinning current diminishes when an exponential or Yukawa-type DW exchange is used to 2.21 and 1.87 A/μm^2, respectively, above $t_s = 0.6$ ns. The variation of the repulsive interaction impacts slightly the shape and surface of the upper bands, the most important change is on the depinning current for the symmetric pulse [panels (a) and (c)]. For asymmetric pulses [panels (e) and (g)], where $t_s = t_f = 5$ ps and the rise time t_r is varied, the change in form and surface of the bands is more important as compared to the symmetric pulses. Increasing the damping parameter α to 0.05 (with $\beta = 2\alpha$) as shown in panels (c) and (g) shifts all the bands to lower currents, including the depinning value. We used in all the calculations the same parameters for the *mm* and *dd* interaction: $a_2 = 0.2$, $a_3 = 0.02$ eV, $D_2 = D_3 = 500$ nm. For the different DW exchange interactions, the parameters used are as follows: $a_1 = 1.2$ eV and $D_1 = 350$ nm for E^H_{exch}, $a_1 = 20$ eV and $D_1 = 150$ nm for $E^{\text{exp}}_{\text{exch}}$ and $a_1 = 90$ eV and $D_1 = 150$ nm for E^Y_{exch}. These parameters were chosen to fit best the micromagnetic depinning line of shortest pulse length. In-depth details about the comparison between analytic and micromagnetic calculations are given in the Supplemental Material [53].

The importance of the pulse shape and length was inferred by decoupling Eqs. (2) [54,55],

$$\ddot{X} = -\frac{\dot{X}}{\tau_d} - \frac{1}{m}\frac{dE}{dX} + \frac{\beta}{\alpha\tau_d}u + \frac{1+\alpha\beta}{1+\alpha^2}\dot{u}, \tag{4}$$

with $m = \frac{2\alpha S\mu_0 M_s \tau_d}{\Delta\gamma_0}$ as the DW mass and $\tau_d = \frac{1+\alpha^2}{\alpha\gamma_0 H_k}$ as the damping time of the wall in the pinning potential. Here, the damping time is 0.27 ns for $\alpha = 0.05$ and 0.68 ns for $\alpha = 0.02$, so the third term in Eq. (4) is more important for higher damping parameter α, resulting in a lower depinning current as observed from Figs. 2(a) and 2(c) (1.85 A/μm^2 compared to 2.60 A/μm^2 for the Heisenberg DW exchange). The depinning current increases to 3.68 A/μm^2 (lowest value) in panel (e) and 3.39 A/μm^2 in panel (g) for a longer rise time as the last term of Eq. (4) is directly proportional to the current derivative. The second term of Eq. (4) gives a hint to the different depinning currents obtained for various DW exchange forms used.

Case of four interacting DWs

The influence of the repulsive interaction between nearest-neighbor DWs was further studied by extending the analytical calculation up to four DWs of same topological charge. We describe, here, the case of a chain of four consecutive interacting DWs: We consider the topological repulsive interaction between first neighbors in the forms presented above, along with the monopole-monopole and dipole-dipole interaction between each pair of DWs. The *mm* and *dd* interactions are attractive between first neighbors, repulsive between second neighbors, and attractive between third neighbors. The parameters a_i and D_i were kept constant for first-, second-, and third-neighbor *mm* and *dd* interactions with the values given above.

Figure 3 displays the influence of the magnitude of the DW exchange interaction between nearest neighbors for

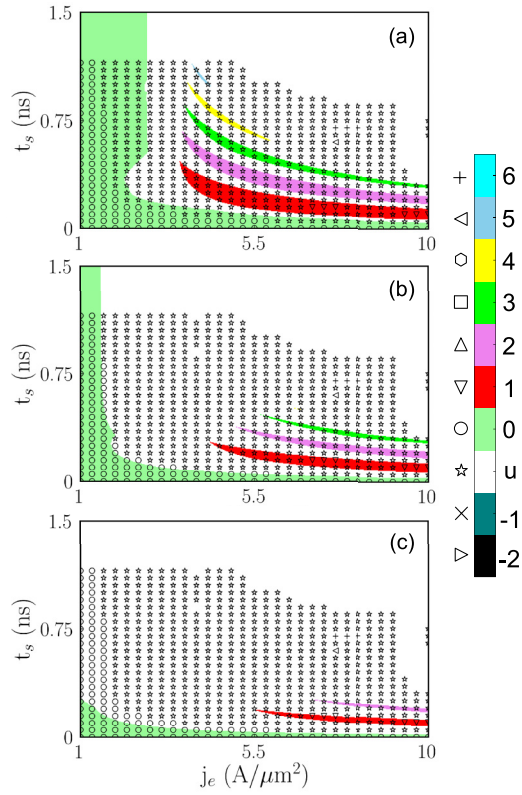

FIG. 3. Influence of the Heisenberg DW exchange energy magnitude on the bands for a train of four neighboring DWs for $\alpha = 0.02$ and $\beta = 0.04$: (a) $a_1 = 0$ eV (no DW exchange), (b) $a_1 = 1.0$ eV and (c) $a_1 = 1.4$ eV. The 1D results (colored regions) obtained for a Heisenberg-type DW exchange interaction are compared with the micromagnetic calculations (scattered symbols) at $T = 0$ K. The pulse stable time was varied with $t_r = t_f = 5$ ps and $t_z = 10$ ns.

$\alpha = 0.02$ using a Heisenberg-type DW exchange. The difference between no DW exchange [panel (a)] and a DW exchange of the same order of magnitude as used for a train of two DWs is much more drastic as the depinning current and the bandwidth diminish strongly when the DW exchange is turned on [panel (b), $a_1 = 1.0$ eV]. A further increase in the DW exchange interaction will lead to the quasisuppression of the depinning current (displaced to lower values), but also of the bands [panel (c), $a_1 = 1.4$ eV]. The analytic results follow very well the micromagnetic ones for the depinning current line [panel (b)] and semiquantitatively the band form, which validates the model.

To further investigate the consequences of the DW exchange interaction type on the DW dynamics, we present the evolution of the phase diagrams in Fig. 4 for different pulse shapes and damping parameters. Panels (a) and (b) show the contour plots of the first bands due to a symmetric current pulse shape ($t_r = t_f = 5$ ps) and for $\alpha = 0.02$ and 0.05, respectively, whereas panels (c) and (d) display the case of asymmetric pulse shape ($t_s = t_f = 5$ ps). In panel (a), the contour plots obtained with the three types of DW exchange interaction are superposed with the results obtained with no repulsive interaction [shown in Fig. 3(a)]. The influence of the different DW exchange forms is more marked for the four

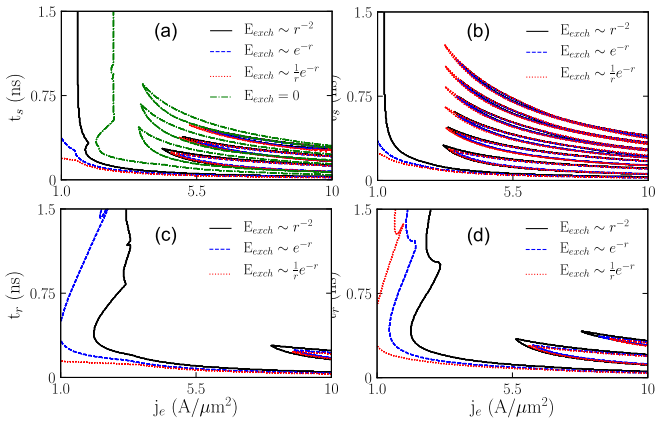

FIG. 4. Contour plots of the different bands obtained for a train of four neighboring DWs (separated by 80 nm) with different types of the DW exchange interaction at $T = 0$ K using the 1D model: (a) and (c) $\alpha = 0.02$ and $\beta = 0.04$, (b) and (d) $\alpha = 0.05$ and $\beta = 0.1$. In (a) and (b), the pulse stable time was varied with $t_r = t_f = 5$ ps, whereas in (c) and (d), the rise time was varied with $t_s = t_f = 5$ ps and $t_z = 10$ ns.

DWs as the depinning current decreases as compared with the two DWs case to 1.54 A/μm^2 for the Heisenberg DW exchange and below 1 A/μm^2 for an exponential or Yukawa-type DW exchange. At the same time, the superior bands are displaced to higher currents as compared to the two-DW case, for example, the beginning of the band +1 to 4.3 A/μm^2 from 3.5 A/μm^2 (the Heisenberg DW exchange). This means that higher currents are needed to achieve a synchronous movement of the DWs and a larger unintended zone. The surface of the bands is also strongly reduced when a Yukawa-type interaction is used, which is the most unfavorable scenario. In the case of the asynchronous current pulse [panels (c) and (d)], the same shift of the depinning current and of the bands is observed with a clear difference between the different DW exchange schemes.

B. Temperature dependence

The effect of temperature was computed with the stochastic 1D model [Eqs. (2)] for the first bands and micromagnetically only on several points that corresponded to the highest probability obtained with the 1D model. A more detailed comparison between the analytic and the micromagnetic calculated probabilities for the first band in Fig. 5(a) is shown in the Supplemental Material [53]. The results obtained analytically at $T = 293$ K are presented in Fig. 5 for a train of two or four DWs. A symmetric current pulse ($t_r = t_f = 5$ ps) was applied after an initial relaxation time of 10 ns followed by another relaxation time of 10 ns. The bands shown in panels (a) and (b) are the bands of Figs. 2(a) and 2(b) for the Heisenberg DW exchange, whereas the bands displayed in panels (c) and (d) are the ones from Figs. 4(a) and 4(b) for the Heisenberg DW exchange. We computed 1000 realizations for the +1 band and 500 realizations for the +2 and +3 bands. The realizations were calculated for half of the points in each band for the train of two DWs [panels (a) and (b)] and for all the band points for the train of four DWs (less total points in the bands).

In Fig. 5(a), the maximum of the probability distribution for the positioning of a train of two DWs to the nearest notch (+1 band) is of 100% obtained for seven states (points) ($\alpha = 0.02$) out of 3093 calculated points with 29.9% of the states having a probability superior of 95%. The states that have 100% probability of desired displacement are obtained for a pulse with $t_s = 100$ ps and current amplitude superior to 9.1 A/μm^2 or $t_s = 110$ ps and $j_e \geqslant 8.5$ A/μm^2. The maximum of probability decays in the superior bands, being of 95.6% on the +2 band and 68.8% on the +3 band. These

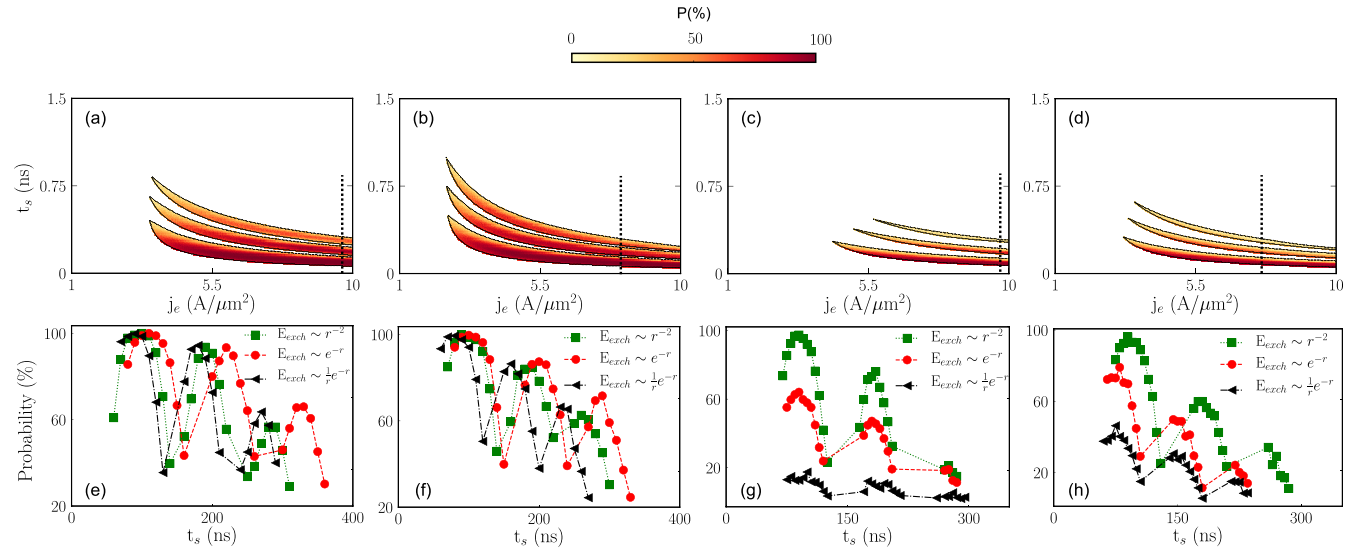

FIG. 5. Probability of DWs motion in different bands at $T = 293$ K for a train of two neighboring DWs and a damping parameter $\alpha = 0.02$ in (a) or $\alpha = 0.05$ in (b) or a train of four neighboring DWs with $\alpha = 0.02$ in (c) or $\alpha = 0.05$ in (d). A Heisenberg-type DW exchange interaction is used along with a nonadiabatic parameter $\beta = 2\alpha$. The vertical dotted lines correspond to the probability profile represented in the figures underneath. The profiles are compared for different types of DW exchange interaction and are chosen in each case as to pass through the maximum probability of the first band (the lowest branch in the figures).

probabilities are comparable with the ones when a single DW is displaced by current pulses [44]. Micromagnetically, the maximum of probability is of 98% (on 100 realizations) obtained for the same pulse characteristics that give maximum probability with the 1D model. The discrepancy is probably due to the small shift of the bands between the two models. For a damping parameter $\alpha = 0.05$ [Fig. 5(b)], the maximum of the probability distribution is 99.9% in the +1 band obtained for a lower current amplitude of 7.8 A/μm^2 and $t_s = 90$ ps. The percentage of states having a probability superior to 95% is of 30.6% of the 3310 calculated states. The maximum of probability is 91% and 77% for the +2 and +3 bands.

For a train of four DWs, the maximum of the probability distribution in the +1 band decreases slowly to 97.4% [$\alpha = 0.02$, panel (c)] and 96.2% [$\alpha = 0.05$, panel (d)]. The probability maximum in the +2 and +3 bands is 76.8% and 28.2%, respectively, for $\alpha = 0.02$ and 70% and 47.8% for the $\alpha = 0.05$ case. The current pulse characteristics for which the probability maximum is obtained are ($t_s = 90$ ps, $j_e = 9.9$ A/μm^2) for $\alpha = 0.02$ and ($t_s = 90$ ps, $j_e = 7.8$ A/μm^2) for $\alpha = 0.05$. The probabilities when an asymmetric pulse is applied are almost equal with the ones obtained for symmetric pulses for all the cases presented above.

In the Figs. 5(e)–5(h), we compare the profiles of the probability distribution when passing through the maximum of the probability in the +1 band for the different DW exchange energies considered. The profiles corresponding to r^{-2} DW exchange are represented by a dotted line in the panels directly above them. There is a considerable difference in the probabilities of a train of two DWs and a train of four DWs: For the two DWs [panels (e) and (f)], the probability maximum is almost the same in the three bands for the different DW exchange interactions with only a shift of the bands along the t_s axis. For the train of four DWs [panels (g) and (h)], the probabilities depend strongly on the spatial variation of the DW exchange interaction. For the $\alpha = 0.02$ case, the maximum probability in the +1 band decreases to 64.1% for the exponential DW exchange and to 17.5% for the Yukawa-type interaction. For $\alpha = 0.05$, the maximum probability is 79.1% for the exponential DW exchange and 46.3% for the Yukawa-type interaction. This difference can be related to the first two terms in Eq. (4), to the damping parameter through the different damping time, and to the force exerted on the walls due to the interaction energy between them. The large difference in probability of the +1 state between the Heisenberg DW exchange and the Yukawa DW exchange is directly imputable to the type of the repulsive energy between the DWs (Supplemental Material [53]), generally the first DW depins even before the application of the current due to the large angular variation and, therefore, large transient effects directly related with the oscillation of the second DW (and their mutual interaction).

C. Influence of transient effects on the DW dynamics

Large transient effects were predicted and observed in the movement of one DW in a nanowire [37,38,44,56]. These transient effects were related to the deformation of the wall in the periodic potential and produced a displacement of the wall in the direction opposite to the STT (opposite to the electron flow), corresponding to negative bands in our phase diagrams. The transient movement was determined to be proportional to the wall angle,

$$\delta X = -\frac{\Delta}{\alpha}\left(1 - \frac{\beta}{\alpha}\right)\delta\psi. \tag{5}$$

The transient displacement was predicted to appear for a value of the nonadiabatic parameter $\beta = 0$, $\beta = \alpha$ and even $\beta = 2\alpha$ for a single DW submitted to ultrashort current pulses [44] comparable with the DW damping time τ_d. In the case of interacting DWs, these transient effects still appear as shown in Fig. 6, but they are greatly reduced (which seem to agree with a quantum-classical hybrid approach [57]). For a train of two DWs, the transient effects appear only for $\beta = 0$ (or close to) when a symmetric pulse is applied (details in the Supplemental Material Ref. [53]) and even for $\beta = 2\alpha$ ($\alpha = 0.02$) for an asymmetric pulse when the rise time is larger than 0.35 ns. However, for a train of four DWs, the transient effects appear only in the case of $\beta = 0$ and a rise time superior of 0.5 ns forming a reduced −1 band. These effects still appear even for a train of five DWs [Fig. 6(i)] with the −1 band shrinking rapidly.

The transient effect appear due to a combination of factors [44]: The presence of the periodic pinning potential which distorts the DWs, restoring force in the potential well, position of the DWs in the potential well at the pulse end, and a low damping value. For the train of four DWs, the walls that are situated at the interior of the train are less distorted than the ones which are situated at the beginning and the end of the sequence as the interior walls fill symmetric interaction forces from both neighboring walls and are situated at the center of the potential well. The exterior walls are more deformed as they are pushed from the equilibrium position of the potential well, and they escape first from the train creating unintended states.

The results obtained with the analytical model for a train of two DWs are displayed in Figs. 6(a)–6(c) for the different DW exchange interactions and different initial distances between the DWs ($\alpha = 0.05$, $\beta = 0$). When the two DWs are initially pinned in nearest-neighboring notches situated 80 nm apart, the −1 band is obtained only for Heisenberg DW exchange and only for currents inferiors to 7.7 A/μm^2. There is a discrepancy with the micromagnetic result shown in panel (d) where the −1 band continue to higher currents for shorter pulse length. If the two DWs are initially pinned at second-neighboring notches 160 nm apart [panel (b)], the −1 band obtained analytically follows closely the micromagnetic one [panel (e)] even though somewhat larger. In this case, the −1 band is obtained also for exponential DW exchange. Furthermore, if the two DWs are pinned initially even further away at third-neighboring notches 240 nm apart [panel (c)], the −1 band is obtained for all three types of DW exchange interaction with almost same bandwidth and form and very close to the micromagnetic result [panel (f)]. As the two DWs are further away, the DW exchange interaction have only a limited influence, and the dipolar interaction determines the form of the bands. We observe that the DW exchange interaction at shorter distances modifies the width and form of the band. For a train of three, four, or five DWs, the −1 band

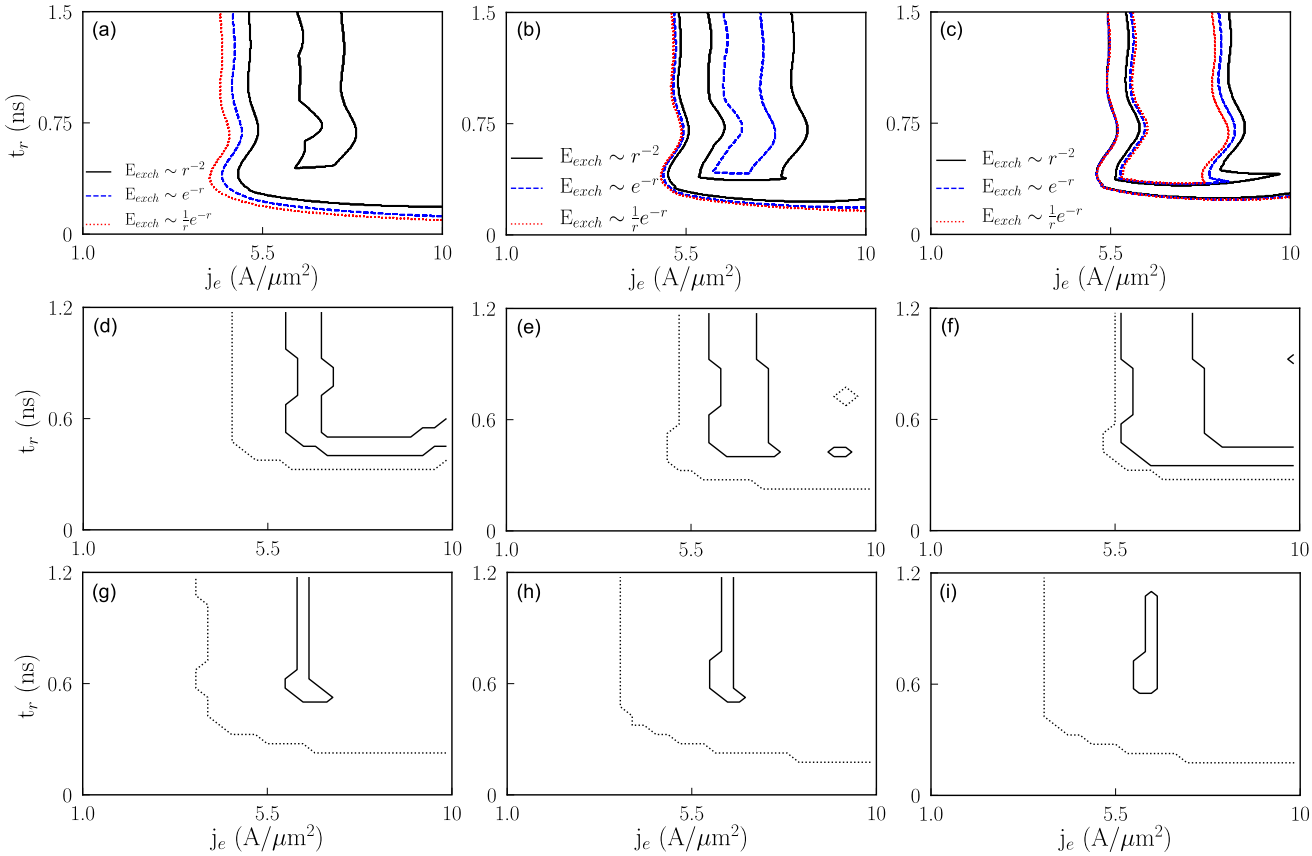

FIG. 6. Influence of the pulse rise time t_r on the phase diagram for a train of several DWs at $T = 0$ K for $\alpha = 0.05$ and $\beta = 0$. The parameter space is the rise time vs current amplitude. In all cases, $t_s = t_f = 5$ ps and $_tz = 10$ ns. The 1D model results for different DW exchange energies are shown in panels (a)–(c) for a train of two DWs separated by (a) 80 nm, (b) 160 nm, and (c) 240 nm. Only the band -1 is visible in the center of the diagram together with the depinning boundary. The micromagnetic results are presented in panels (d)–(i) where band -1 is represented by a continuous line and the limit of band 0 is represented by the dotted line. The micromagnetic simulations are for a train of two DWs separated by: (d) 80 nm, (e) 160 nm, and (f) 240 nm and a train of (g) three DWs, (h) four DWs, and (i) five DWs separated by 80 nm.

is still obtained micromagnetically as shown in the panels (g)–(i). Analytically, we did not obtain the -1 band for neither of the DW exchange interactions for trains of DWs superior of two and the parameters used above. This can be related to the smallness of the bands width and to the values of the DW exchange parameters, but also to the pinning potential analytical description (harmonic periodic potential). Changing the DW exchange parameters allows to obtain the negative bands, but the depinning line no longer follows the micromagnetic result and differences are obtained for the others values of α and β. The values for the DW exchange and dipolar parameters were chosen to follow closely the depinning line and the first bands for $\beta = 2\alpha$. These parameters give semiquantitative results even for $\beta = 0$ (the depinning line, for example), but the limit of the 1D model is reached.

IV. DISCUSSION AND CONCLUSION

We investigated the repulsive interaction between transverse DWs with the same topological charge, pinned at constrictions in a magnetic nanowire. Our analytical study of the DW interaction shows that a r^{-2} decay describes best the micromagnetic results. The same power-law variation was found to describe the vortex-vortex interaction in superconducting films [7] but differs from the vortex-vortex interaction in bulk superconductors or the magnetic vortex-vortex interaction calculated in a 2D anisotropic film (which decays logarithmically). Our trial functions for the interaction potential also included an exponential or Yukawa potential, which describe a large number of interaction forces in many areas of condensed-matter physics (in discrete or continuum models).

The analytical phase diagrams for a train of up to four DWs follow closely the ones calculated with micromagnetic simulations when the r^{-2} decay is used. If the repulsive interaction would decay with an Yukawa potential, the changes to the phase diagrams are important starting from the depinning current and the form of the bands to the large decrease in the maximum jump probability to the nearest pinning position (the $+1$ band) at room temperature and the suppression of the transient effects. The Yukawa-type repulsive interaction between DWs is the most unfavorable scenario for the collective motion of DWs in a nanostrip at room temperature.

A train of four DWs is shown to be displaced regularly between pinning centers with ultrashort current pulses (100 ps), leading to practical applications, such as magnetic

memories. The lowest depinning currents are found for the ultrashort rise time of the pulse as described before [44] as long as the largest bandwidth. When going from a train of two nearest-neighboring DWs to a train of four, the main impact is the decrease in the depinning current, but, at the same time, a decrease in the bandwidth and an increase in the unintended region with larger transition regions between the bands. The transient effects are also severely diminished due to the mutual interaction and are eventually suppressed.

We would like to discuss our results on the repulsive interaction between DWs from the spin waves perspective. The spin waves or magnons are the elementary excitations of the electronic magnetic system [58], quasiparticles with a $\hbar$ angular momentum, and $\hbar k$ linear momentum. It was shown both theoretically [59–64] and experimentally [65] that the spin waves can induce DW motion in both directions due to the angular or linear momentum transfer. The motion is directly related with the transmission coefficient of the spin waves passing through the wall. It was also shown numerically that the rigid DW motion is not stable against spin wave emission [66–69]. In principle, a DW submitted to an ultrashort current pulse could emit spin waves that interact with other DWs. This interaction will be attractive if only the angular momentum is transferred to the second DW (magnonic spin torque) or more complex if linear momentum is also transferred. The repulsive interaction considered here is thought to be mediated through the exchange of gauge bosons of integer spin which could be virtual magnons. A DW would emit a magnon that is absorbed by another DW of opposite topological charge, therefore, inducing the repulsive interaction which is a fundamental interaction that exists with or without the presence of notches or an applied external current. If the DWs could rotate out of plane, one of the DWs could change its topological charge, and the interaction can become attractive as observed in cylindrical nanowires [15]. In our view, this can be demonstrated exactly only in a microscopic theory and cannot be proved in a continuum theory. In our micromagnetic simulation, this interaction arises due to the exchange energy term and is described analytically, such as an exchange interaction between DWs (which can be described as a magnon spin current).

To summarize, our calculations show that an analytical description of the interaction between several DWs is possible paving the way for larger calculations of interacting DWs in nanowires. We expect the same type of dependence to take place between Bloch or Néel DWs in thin films with perpendicular magnetic anisotropy.

ACKNOWLEDGMENTS

This work was granted access to the HPC resources of Aix-Marseille Université financed by the project Equip@Meso (Grant No. ANR-10-EQPX-29-01) of the program "Investissements d'Avenir" supervised by the Agence Nationale pour la Recherche.

[1] R. Machleidt and I. Slaus, J. Phys. G: Nucl. Part. Phys. **27**, R69 (2001).
[2] P. K. Shukla and K. Avinash, Phys. Rev. Lett. **107**, 135002 (2011).
[3] K. Kremer, M. O. Robbins, and G. S. Grest, Phys. Rev. Lett. **57**, 2694 (1986).
[4] R. Boesch, P. Stancioff, and C. R. Willis, Phys. Rev. B **38**, 6713 (1988).
[5] H. B. Nielsen and P. Olesen, Nucl. Phys. B **61**, 45 (1973).
[6] M. B. Hindmarsh and T. W. B. Kibble, Rep. Prog. Phys. **58**, 477 (1995).
[7] A. L. Fetter and P. C. Hohenberg, Phys. Rev. **159**, 330 (1967).
[8] D. Helbing, Rev. Mod. Phys. **73**, 1067 (2001).
[9] W. F. Brown, *Micromagnetics* (Interscience, New York, London, 1963).
[10] R. D. McMichael and M. J. Donahue, IEEE Trans. Magn. **33**, 4167 (1997).
[11] J. M. Kosterlitz and D. J. Thouless, J. Phys. C: Solid State Phys. **6**, 1181 (1973).
[12] O. Tchernyshyov and G.-W. Chern, Phys. Rev. Lett. **95**, 197204 (2005).
[13] S. K. Kim, S. Takei, and Y. Tserkovnyak, Phys. Rev. B **92**, 220409(R) (2015).
[14] S. B. Braun, Adv. Phys. **61**, 1 (2012).
[15] V. O. Dolocan, Eur. Phys. J. B **87**, 188 (2014).
[16] A. Pushp, T. Phung, C. Rettner, B. P. Hughes, S.-H. Yang, L. Thomas, and S. S. P. Parkin, Nat. Phys. **9**, 505 (2013).
[17] S. S. P. Parkin, M. Hayashi, and L. Thomas, Science **320**, 190 (2008).
[18] D. A. Allwood, G. Xiong, C. C. Faulkner, D. Atkinson, D. Petit, and R. P. Cowburn, Science **309**, 1688 (2005).
[19] A. R. Völkel, F. G. Mertens, A. R. Bishop, and G. M. Wysin, Phys. Rev. B **43**, 5992 (1991).
[20] A. R. Völkel, G. M. Wysin, F. G. Mertens, A. R. Bishop, and H. J. Schnitzer, Phys. Rev. B **50**, 12711 (1994).
[21] K. S. Buchanan, P. E. Roy, M. Grimsditch, F. Y. Fradin, K. Yu. Guslienko, S. D. Bader, and V. Novosad, Nat. Phys. **1**, 172 (2005).
[22] A. Thiaville and Y. Nakatani, in *Spin Dynamics in Confined Magnetic Structures III*, edited by B. Hillebrands, and A. Thiaville (Springer, Berlin, 2006).
[23] M. Kläui, J. Phys.: Condens. Matter **20**, 313001 (2008).
[24] J. Shibata, G. Tatara, and H. Kohno, J. Phys. D: Appl. Phys. **44**, 384004 (2011).
[25] T. J. Hayward, M. T. Bryan, P. W. Fry, P. M. Fundi, M. R. J. Gibbs, M.-Y. Im, P. Fischer, and D. A. Allwood, Appl. Phys. Lett. **96**, 052502 (2010).
[26] T. J. Hayward, M. T. Bryan, P. W. Fry, P. M. Fundi, M. R. J. Gibbs, D. A. Allwood, M.-Y. Im, and P. Fischer, Phys. Rev. B **81**, 020410(R) (2010).
[27] J.-S. Kim, M.-A. Mawass, A. Bisig, B. Kruger, R. M. Reeve, T. Schulz, F. Buttner, J. Yoon, C.-Y. You, M. Weigand, H. Stoll, G. Schutz, H. J. M. Swagten, B. Koopmans, S. Eisebitt, and M. Klaui, Nat. Commun. **5**, 3429 (2014).

[28] A. T. Galkiewicz, L. O'Brien, P. S. Keatley, R. P. Cowburn, and P. A. Crowell, Phys. Rev. B **90**, 024420 (2014).
[29] V. O. Dolocan, Appl. Phys. Lett. **105**, 162401 (2014)
[30] K. Y. Guslienko, J. Nanosci. Nanotechnol. **8**, 2745 (2008).
[31] N. Hasegawa, S. Sugimoto, H. Fujimori, K. Kondou, Y. Niimi, and Y. Otani, Appl. Phys. Express **8**, 063005 (2015).
[32] L. O'Brien, A. Beguivin, D. Petit, A. Fernandez-Pacheco, D. Read, and R. P. Cowburn, Philos. Trans. R. Soc. London, Ser. A **370**, 5794 (2012).
[33] L. Thomas, M. Hayashi, R. Moriya, C. Rettner, and S. S. P. Parkin, Nat. Commun. **3**, 810 (2012).
[34] B. Krüger, J. Phys.: Condens. Matter **24**, 024209 (2012).
[35] A. Pivano and V. O. Dolocan, J. Magn. Magn. Mater. **393**, 334 (2015).
[36] J. M. Kosterlitz, J. Phys. C: Solid State Phys. **7**, 1046 (1974).
[37] A. Thiaville, Y. Nakatani, F. Piechon, J. Miltat, and T. Ono, Eur. Phys. J. B **60**, 15 (2007).
[38] J. Y. Chauleau, R. Weil, A. Thiaville, and J. Miltat, Phys. Rev. B **82**, 214414 (2010).
[39] L. Thomas, M. Hayashi, X. Jiang, R. Moriya, C. Rettner, and S. S. P. Parkin, Nature (London) **443**, 197 (2006).
[40] L. Thomas, R. Moriya, C. Rettner, and S. S. P. Parkin, Science **330**, 1810 (2010).
[41] J. Rhensius, L. Heyne, D. Backes, S. Krzyk, L. J. Heyderman, L. Joly, F. Nolting, and M. Kläui, Phys. Rev. Lett. **104**, 067201 (2010).
[42] E. Martinez, L. Lopez-Diaz, O. Alejos, L. Torres, and M. Carpentieri, Phys. Rev. B **79**, 094430 (2009).
[43] H. Y. Yuan and X. R. Wang, Phys. Rev. B **89**, 054423 (2014).
[44] A. Pivano and V. O. Dolocan, Phys. Rev. B **96**, 224431 (2017).
[45] J. C. Slonczewski, J. Appl. Phys. **45**, 2705 (1974).
[46] A. Vansteenkiste, J. Leliaert, M. Dvornik, M. Helsen, F. Garcia-Sanchez, and B. Van Waeyenberge, AIP Adv. **4**, 107133 (2014).
[47] S. Zhang and Z. Li, Phys. Rev. Lett. **93**, 127204 (2004).
[48] O. Boulle, G. Malinowski, and M. Kläui, Mater. Sci. Eng., R **72**, 159 (2011).
[49] M. E. Lucassen, H. J. van Driel, C. M. Smith, and R. A. Duine, Phys. Rev. B **79**, 224411 (2009).
[50] H. Y. Yuan and X. R. Wang, J. Magn. Magn. Mater. **368**, 70 (2014).
[51] H. Y. Yuan and X. R. Wang, Phys. Rev. B **92**, 054419 (2015).
[52] K. Gilmore, Y. U. Idzerda, and M. D. Stiles, Phys. Rev. Lett. **99**, 027204 (2007).
[53] See Supplemental Material at http://link.aps.org/supplemental/10.1103/PhysRevB.101.014438 for details of parameters influence on phase diagram.
[54] B. Krüger, D. Pfannkuche, M. Bolte, G. Meier, and U. Merkt, Phys. Rev. B **75**, 054421 (2007).
[55] L. Bocklage, B. Krüger, T. Matsuyama, M. Bolte, U. Merkt, D. Pfannkuche, and G. Meier, Phys. Rev. Lett. **103**, 197204 (2009).
[56] J. Vogel, M. Bonfim, N. Rougemaille, O. Boulle, I. M. Miron, S. Auffret, B. Rodmacq, G. Gaudin, J. C. Cezar, F. Sirotti, and S. Pizzini, Phys. Rev. Lett. **108**, 247202 (2012).
[57] M. D. Petrovic, B. S. Popescu, U. Bajpai, P. Plechac, and B. K. Nikolic, Phys. Rev. Appl. **10**, 054038 (2018).
[58] A. G. Gurevich and G. A. Melkov, *Magnetization Oscillations and Waves* (CRC Press, Boca Raton, New York, London, 1996).
[59] D.-S. Han, S.-K. Kim, J.-Y. Lee, S. J. Hermsdoerfer, H. Schultheiss, B. Leven, and B. Hillebrands, Appl. Phys. Lett. **94**, 112502 (2009).
[60] M. Jamali, H. Yang, and K.-J. Lee, Appl. Phys. Lett. **96**, 242501 (2010).
[61] P. Yan, X. S. Wang, and X. R. Wang, Phys. Rev. Lett. **107**, 177207 (2011).
[62] J.-S. Kim, M. Stark, M. Klaui, J. Yoon, C.-Y. You, L. Lopez-Diaz, and E. Martinez, Phys. Rev. B **85**, 174428 (2012).
[63] X.-G. Wang, G.-H. Guo, Y.-Z. Nie, G.-F. Zhang, and Z.-X. Li, Phys. Rev. B **86**, 054445 (2012).
[64] P. Yan, A. Kamra, Y. Cao, and G. E. W. Bauer, Phys. Rev. B **88**, 144413 (2013).
[65] W. Jiang, P. Upadhyaya, Y. Fan, J. Zhao, M. Wang, L.-T. Chang, M. Lang, K. L. Wong, M. Lewis, Y.-T. Lin, J. Tang, S. Cherepov, X. Zhou, Y. Tserkovnyak, R. N. Schwartz, and K. L. Wang, Phys. Rev. Lett. **110**, 177202 (2013).
[66] D. Bouzidi and H. Suhl, Phys. Rev. Lett. **65**, 2587 (1990).
[67] J. Fernandez-Rossier, M. Braun, A. S. Nunez, and A. H. MacDonald, Phys. Rev. B **69**, 174412 (2004).
[68] X. S. Wang, P. Yan, Y. H. Shen, G. E. W. Bauer, and X. R. Wang, Phys. Rev. Lett. **109**, 167209 (2012).
[69] B. Hu and X. R. Wang, Phys. Rev. Lett. **111**, 027205 (2013).